Application of Transformation Optics and Metamaterials: Enhancing Utilization of Optical Device

By Gyushik Jang

Adviser: Dr. David Smith

Submitted 4/20/2011

Duke University

Department of Electrical and Computer Engineering

TABLE OF CONTENT

APPLICATION OF TRANSFORMATION OPTICS AND METAMATERIALS: ENHANCING UTILIZATION OF OPTICAL DEVICE

I. ABSTRACT 3
II. INTRODUCTION 4
III. EXPERIMENT AND ANALYSIS 6
IV. CONCLUSION AND FUTURE WORK 13
V. ACKNOWLEDGEMENT 14
VI. REFERENCES 14
VII. APPENDIX 16

I. Abstract

The objective of this research is to design an advanced optical device employing transformation optics. The design involving gradient index is realized using metamaterials, and the behavior is verified at microwave frequencies with experiment and data analysis. The device studied is Maxwell lens, which is a near-perfect relay lens with a flattened focal surface designed to reduce spherical ray aberration normally associated with the conventional fish-eyed lens. The electric field distributions that reveal the ray trajectories within the lens are obtained with the use of 2D mapper, and analysis on the data demonstrates the behaviors of the flattened fish-eyed lens are consistent with the simulation. This research demonstrates a practical possibility of the implementation of transformation optics and metamaterials in such fields as photonics and chip-based systems where metamterials can be introduced as an alternative method to build waveguides.

II. Introduction

Metamaterials

In electromagnetic devices, waves enter the medium and interact with the constituent atoms and molecules of the material. The manipulation of these electromagnetic waves, which can range from wavelengths of a few nanometers to thousands of kilometers, is determined by the way the electric and magnetic fields of the waves alter the electrons within the material. Although this precise mechanism by which optical devices controls the light is well-understood, the implementation of creative ideas exploiting this principle has been limited due to the narrow range of electromagnetic properties available in naturally occurring or chemically synthesized materials. Electromagnetic metamaterials are artificially structured composites that have gained considerable attention for its capability to broaden this range of properties. Metamaterials, effectively simulating a homogenous material by putting together a two-dimensional array of copper strips, has been successful in illustrating a wide variety of interesting concepts and implementations such as negative index of refraction, broadband wave retarder, arbitrarily shaped concentrators, and even invisibility cloaks [1-4].

One area of metamaterials implementation that can have significant impact on the microelectric field is in integrated-circuit design. It has been proposed that waveguide left-handed metamaterial medium can be incorporated to radio frequency/monolithic microwave integrated circuit (RF/MMIC) with potential to miniaturize circuits and simplified fabrication steps[5,6]. In this research, we examine the applicability of metametarials in modifying the electromagnetic response of a conventional optical device. A concept device, Maxwell lens, is constructed, and this device can potentially propose a new design for chip-integrated waveguides. Maxwell lens is an advanced optical device that aims to enhance the utility of fish-eye lens. Although the unique characteristic of a fish-eye lens, which relays an incident light to its conjugate side, can serve as a special type of waveguide, its spherical shape introduces an inherent geometrical aberration that rids much of its utilizable behaviors. The design object of Maxwell lens therefore is to flatten the focal surfaces of a fish-eye lens in order to minimize the ray aberration. The index profile of conventional fish-eye lens can be expressed as follows

$$n(r) = \frac{n_0}{1+(r/a)^2}$$

Equation 1

where a is the radius and n_0 is the index of refraction at the center. The ray trajectories for a spherical region with the given index profile have been simulated using Mathematica[7] as shown in Figure 1. The coordinate transformation used to flatten the focal surface[7]

$$x'(x,z) = \frac{w}{a}x$$

$$z'(x,z) = \frac{zl}{\sqrt{a^2 - x^2}}$$

Equation 2

distorts the cylindrical region of radius a to a rectangular region of width w and height l, and the simulated ray trajectories in the new coordinate system are shown in Figure 1.

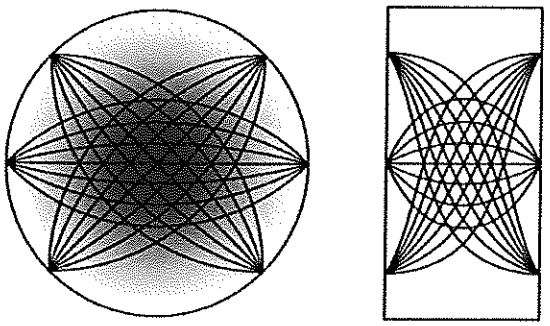

Figure 1: Demonstration of ray trajectories in conventional fish-eyed lens (left) vs in transformed lens (right) [4]

Transformation Optics

Transformation optics is a design approach used in optics and electromagnetics to achieve specific spatial distribution of gradient index. The technique is based on form invariance of Maxwell's equation, which can describe the same wave solution in different coordinate systems to the extent that the tensor elements of the constitutive parameters, electric permittivity (ε) and magnetic permeability (μ), can be expressed as functions of the system coordinates. The TO first applies a coordinate transformation to a region of space. The coordinate transformation does not change the wave solution that defines the space in its original coordinate, although the solution will appear distorted relative to the original coordinate system. The transformation can be used to design a specific medium where the wave paths are manipulated, thus characterizing an optical device. Also, it is important that the particular coordinate transformation obtained with the TO method results in achievable configurations of the medium where the constitutive parameters are isotropic and within obtainable range. The parameters can be found using the equations[7]

$$\varepsilon' = \frac{\Lambda\varepsilon\Lambda^T}{|\Lambda|}n^2(x,z)$$

$$\mu' = \frac{\Lambda\varepsilon\Lambda^T}{|\Lambda|}$$

Equation 3

where $n(x,z)$ is the initial index distribution of the fish-eye lens and Λ is the Jacobian matrix given in Equation 4(a).

$$\Lambda = \begin{pmatrix} \frac{\partial x'}{\partial x} & \frac{\partial x'}{\partial y} & \frac{\partial x'}{\partial z} \\ \frac{\partial y'}{\partial x} & \frac{\partial y'}{\partial y} & \frac{\partial y'}{\partial z} \\ \frac{\partial z'}{\partial x} & \frac{\partial z'}{\partial y} & \frac{\partial z'}{\partial z} \end{pmatrix} \quad \text{(a)} \qquad \Lambda = \begin{pmatrix} \frac{\partial x'}{\partial x} & \frac{\partial x'}{\partial y} & 0 \\ \frac{\partial y'}{\partial x} & \frac{\partial y'}{\partial y} & 0 \\ 0 & 0 & 1 \end{pmatrix} \quad \text{(b)}$$

Equation 4

For more achievable material properties, the optimization technique known as quasi-conformal transformation optics (QCTO) can be applied to minimize the inhomogeneity and anisotropy of the tensor elements, thereby reducing the complexity of the medium. The QCTO method begins by simplifying the Jacobian matrix to Equation 4(b) assuming a two-dimensional transformation only within the x-y plane and the electric field polarized along z-axis. Defining and manipulating a function that measures the degree of anisotropy [8], the method can yield a set of nonlinear partial differential equations solvable for $x'(x,y)$ and $y'(x,y)$

$$\frac{\partial^2 x'}{\partial x^2} + \frac{\partial^2 y'}{\partial y^2} = 0$$

$$\frac{\partial^2 y'}{\partial x^2} + \frac{\partial y'}{\partial y^2} = 0$$

Equation 6

Solving the equations with appropriate boundary conditions such as *Neumann-Dirichlet* or *Dirichlet* conditions illustrates the optimization applied to determine the transformation grid for the fish-eye lens (Figure 2).

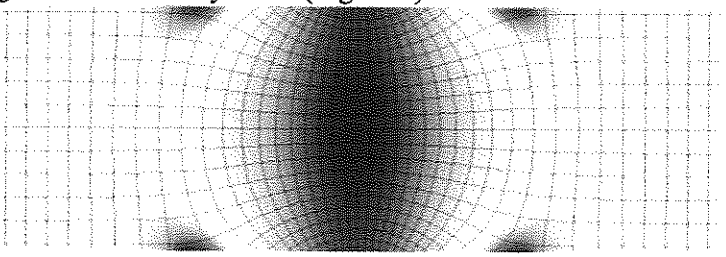

Figure 2: Permittivity distribution corresponding to the flattened fish-eye lens[7]

III. Experiment and Analysis

Fabrication

The fabrication of the flattened fish-eyed lens starts with the mask generated using a MATLAB script that draws the dipoles and cutouts based on the transformed index profile, which is computed using the technique described in the previous section. The composite used to construct the device is FR-4 (Flame, Retardancies, #4 epoxy), a dielectric fiberglass epoxy resin sheet, pre-coated with a layer of copper on one side or both. The mechanical strength and electrical insulating qualities of FR-4 make it a versatile material suitable for various electrical applications.

Figure 3: UV Light Exposure

1. Exposure of FR-4 to UV light

The mask is put on top of the FR4 sheet, and the sheet is exposed to UV light for 25 seconds to harden the photoresist (Figure 3). The negative photoresist, also pre-coated on FR-4, hardens when exposed to light.

2. Developing photoresist

The sheet is developed with the solution containing 30% sodium hydroxide and tap water. This removes the unexposed resist that is not hardened in the previous step, leaving the photoresist only on the part of the sheet where dipoles will be formed.

3. Etching

The removal of the unexposed resist during development step exposes the copper underneath the resist. This copper is then etched with ferric chloride.

4. Resist removal

The hardened photoresist is washed away with acetone, leaving the sheet containing only the regions of copper that is either etched or intact.

5. Cutting out index and strips

Milling machine is used to cutout each strip and also to make the low index cutout region of air.

6. Assembling of strips

The individual strips are inserted on three vertical strips that act as a holder. The assembled lens is shown in Figure 4.

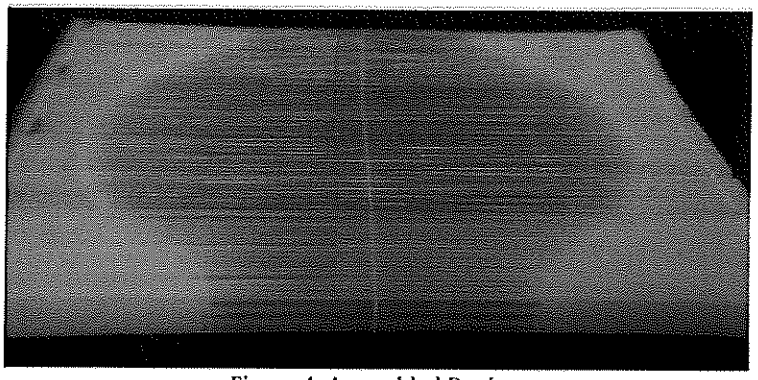

Figure 4: Assembled Device

Experimental Set-up

The approach used to confirm the behavior is to feed in an incident light at different points of one side of the lens and observe the ray trajectories within the lens. 2D mapper is used to obtain the two-dimensional full view of the field map required for such analysis. 2D mapper consists of two horizontal parallel plates spaced 11 mm apart. The light source, coax-to-waveguide adaptor, is attached at the bottom plate and allows the introduction of microwave of varying frequencies (8GHz~13GHz) into the field between the plates [9]. This input microwave is incident on Maxwell lens, which is placed at the center of the bottom plate, through a dielectric waveguide feed (Figure 5). Saw-tooth microwave absorber is placed circularly surrounding the lens to prevent the microwave from reflecting back into the mapped area (Figure 5), thus emulating an infinite two-dimensional parallel plate. A set of six field-sensing antennas is inserted at the upper plate of the mapper. By stepping the lower plate at an increment of 3mm and recording the field amplitude and phase at each step with the antennas at the upper plate, the mapper gathers the phase and amplitude for the entire spatial distribution of electric field within and outside the lens. The experiment is repeated with the guided microwave entering the lens at five different positions from one end to the other. Since the light

source is fixed at a constant position, the lens is moved instead at an increment of 11mm for a total of five times between one end of the input to the other end, which is 55mm.

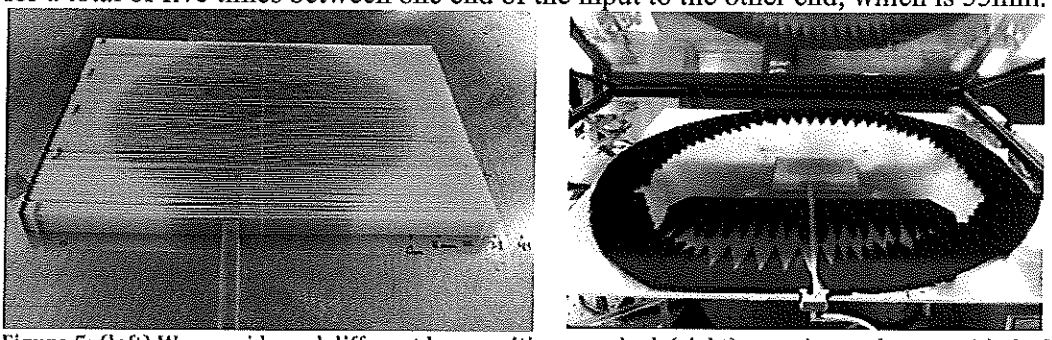

Figure 5: (left) Wave guide and different lens positions marked, (right) experimental setup with the lens on 2D Mapper

Field Distribution Analysis

The raw data gathered with 2D mapper is translated using MATLAB to visualize the field distribution. The frequency of the microwave used in this experiment ranges from 8GHz to 13GHz. The wavelength at the lower bound of the frequency range is then 37.5mm. Considering that the diameter of the lens is 150mm, 8GHz is appropriate because it is small enough to allow the light to interact with the internal structure of the device and the focal points to lie within the lens. The upper bound is established to maintain the homogenization of the device such that the composite structure can be viewed as one solid block of a material from an electromagnetic perspective. The wavelength of the light should be long enough to cover at least ten unit cells, and since the thickness of each unit cell layer is 1.5mm, we have

$$f = \frac{c}{\lambda} = \frac{3 \times 10^8}{(1.5 \times 10^{-3}) \times 10} = 20GHz$$

Figure 6 shows the field map of the same incident light position at different frequencies, and it is observed that the plots properly demonstrate the lens behavior, although more background radiation is seen at 8GHz. For consistency, 12GHz is used for rest of the analysis.

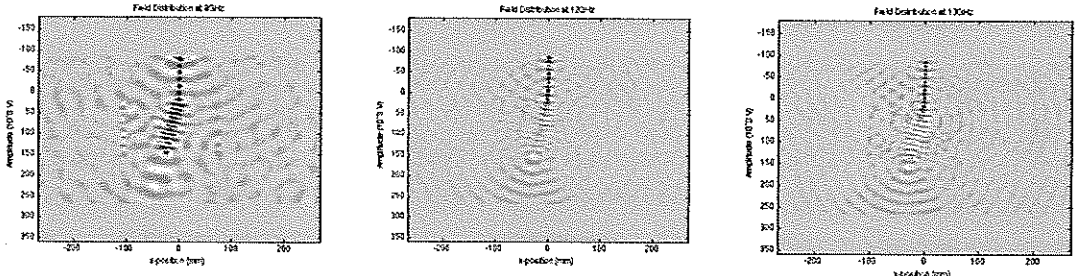

(a) (b) (c)

Figure 6: Field Distributions at (a)8GHz, (b)12GHz, and (c) 13GHz

Comparing the field maps at different positions first requires normalization. This is because it is the lens, not the light source, that is shifted horizontally during the data collection. Thus, the region of interest in all of the five field maps relative to the lens position is selected, and the exact location of the lens is recognized. This allows for more

intuitive demonstration of the ray trajectories for different incident positions when the cropped streams are put together. Figure 8 shows the incident light entering the lens at the upper side and exiting conjugate side at the bottom. The field distribution is consistent with the simulation (Figure 7), and it can also be noted that there is not significant amount of standing waves in the experimented data.

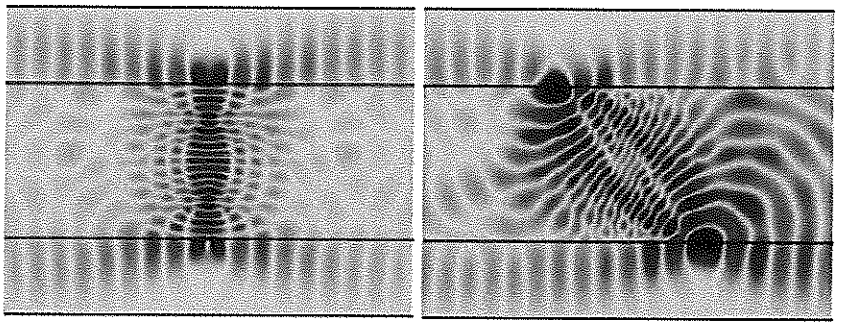

Figure 7: Simulations of fish-eyed lens[7]

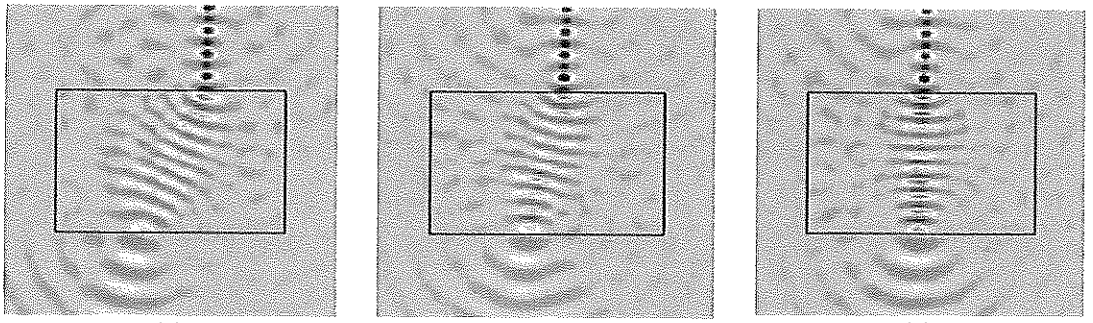

(a) (b) (c)

(d) (e)

Figure 8: Stream of Field Distributions at Different Incident Positions (click to watch the movie)

Cross-section Analysis

In order to take a closer look at the lens behaviors within the mapped region, the power distributions at the cross-sections the lens at both input and output boundary are analyzed. This can demonstrate the relay property of the Maxwell lens as well as the subsequent power loss over the medium. If we use $\alpha_m = f\alpha_{fr-4}$ to denote the loss tangent of each unit cell where f is the volume fraction of the FR-4 strip (f = 0.2/1.5) within a unit cell and α_{fr-4} is the loss tangent (0.025) of FR-4, the electric field can be expressed as

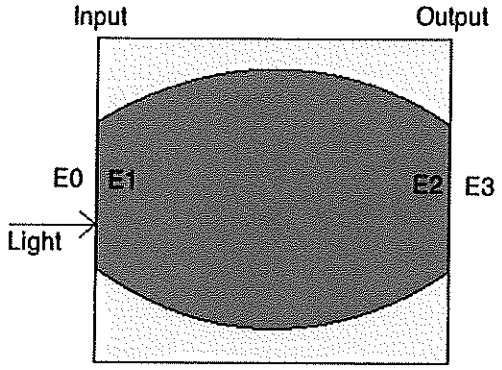

Figure 9: Electric fields near lens boundaries

$$E_2 = E_0 e^{ikx} e^{-\alpha_m \theta}$$

Equation 3

assuming that the impedance mismatch is negligible at each boundary of the lens such that E_1=E_0 and E_2=E_3 (Figure 9). In this equation, ϑ is the wavenumber for light in the lens. Since the refractive index changes over the lens, ϑ can be computed by integrating over the diameter of the lens

$$\vartheta = \int_{-a}^{a} K_0 n(r) dr$$

$$K_0 = \frac{2\pi}{\lambda}$$

Equation 4

where a is the radius of the lens and $n(r)$ is given in Equation 2. The reduction of the electric field amplitude over the lens can be found

$$\left|\frac{E_2}{E_0}\right| = e^{-\alpha_m \theta}$$

Equation 5

and it follows that the power loss is predicted to be 17.91%.

Initially, the power distributions at the closest cross-sections 3mm inside and outside of the lens are measured (Figure 10) to examine the intensities across the boundary. On the external cross-sections, the overall distribution trend shown in the plots is fairly consistent with the expectation. On average, the positions of the output peaks are off by 3.63mm assuming that the wave should travel to the exact conjugate side from which it entered the lens. The power loss is 66.24% as the light enters the lens, travels through the multi-layers of FR-4 strips and exits the lens. On the other hand, the internal cross-sections reveal a puzzling plot with the average location of the output peaks off by 8.34mm. This is evident in the second lens position, which randomly appears on wrong sides of the output boundary. Also, the negative average power loss of -67.22% clearly indicates misrepresented data. In an effort to minimize the bias that arises from choosing a cross-section that is dominated by the standing wave interference, total of 10 cross-sections, 5 at each end of the lens (Figure 11), are sampled and averaged.

Position(mm)	22	11	0 (center)	-11	-22
Pin (10^{-5})	1.002	0.084	0.061	0.169	0.524
Pout(10^{-5})	0.232	0.236	0.212	0.161	0.474
Loss (%)	76.91	-180.5	-246.6	4.5	9.6

(a) Internal cross-section ($Loss_{avg}$ = -67.22%)

Position(mm)	22	11	0 (center)	-11	-22
Pin (10^{-5})	1.720	1.098	0.945	0.856	0.854
Pout(10^{-5})	0.451	0.351	0.296	0.297	0.405
Loss (%)	76.77	68.07	68.7	65.34	52.34

(b) External cross-section ($Loss_{avg}$ = 66.24%)

Table 1: Power loss over the lens for (a) internal and (b) external cross-sections

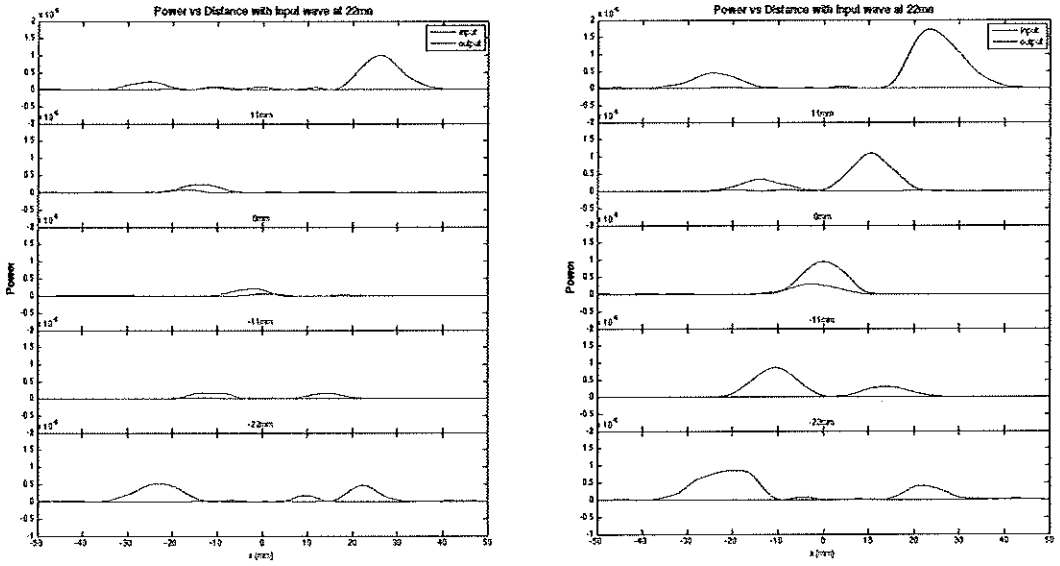

Figure 10: Power Distribution for cross-sections 3mm outside(left) and inside(right) of the lens

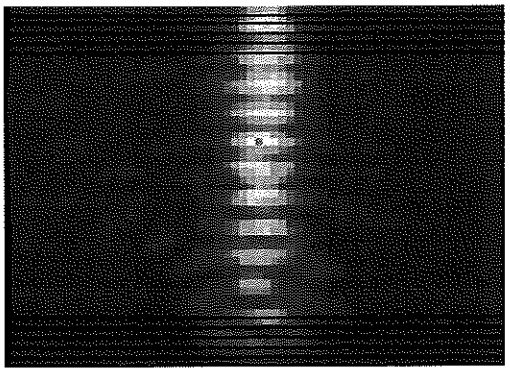

Figure 11: Power distribution and five sample cross-sections

Figure 12 shows the average power distribution at five different inward cross-sections. In the case of average cross-sections, the positions of the output peaks differ from the expected result by 2.06mm and 3.29mm for internal and external sections, respectively. And the average power loss in the internal cross-sections is 49.70%, whereas the loss in a region encompassing the entire lens area is 84.58% (Table 2). The difference between the two values is because the source light intensity is reduced as it leaves the dielectric waveguide and starts to radiate out. Compared with the theoretical loss of 17.81%, the internal power loss of 49.70% is greater because the ray gets defocused as it travels within the medium. To compensate for the wider peaks near the output boundaries, the sum of the intensity values over the wider output areas can be inspected and compared with that over the input areas. The loss is then 35.32% and 69.07% for internal and external cross-sections, respectively. This remaining difference attributes to the fact that the lens boundaries are not precisely impedance-matched with the surrounding. It is very likely that the waves are reflected each time it encounters a boundary resulting in a significant power loss when the steady state is reached.

Position(mm)	22	11	0 (center)	-11	-22
Pin (10^{-5})	0.621	0.475	0.315	0.274	0.358
Pout(10^{-5})	0.295	0.142	0.190	0.159	0.200
Loss (%)	52.49	70.18	39.73	41.59	44.5

(a) Internal cross-section ($Loss_{avg}$ = 49.70%)

Position(mm)	22	11	0 (center)	-11	-22
Pin (10^{-5})	1.155	1.111	0.984	0.863	1.071
Pout(10^{-5})	0.238	0.152	0.150	0.151	0.164
Loss (%)	84.69	86.21	84.78	82.56	84.68

(b) External cross-section ($Loss_{avg}$ = 84.58%)

Table 2: Average power loss over the lens for (a) internal and (b) external cross-sections

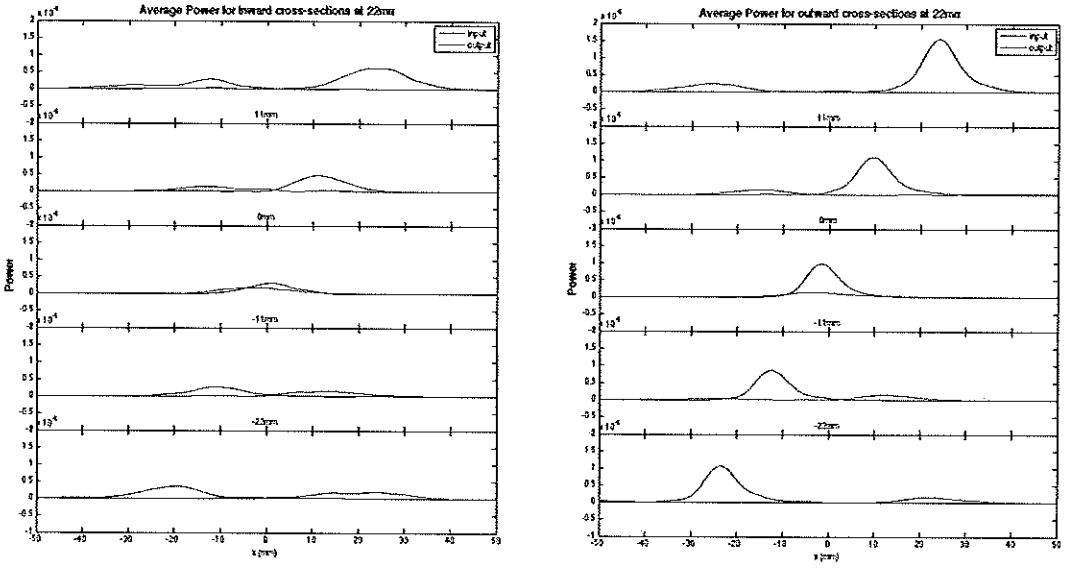

Figure 12: Average Cross Section Plots for internal cross-sections(left) and external cross-sections(right)

The experimental data still yields solid evidence to achieve the main aim of this study, which is to demonstrate the applicability of transformation optics with regards to its capability to manipulate the pathways of a wave. However, if one were to advance the design of Maxwell lens, several options can be considered to minimize the impedance mismatch and thus the power loss. One is to use a more reliable and low-loss substrate such as R/T Duroid or glass microfiber Teflon that have lower loss tangents. The loss tangent of FR-4 substrate, although often used for its flexibility and relatively cheaper cost, is inconsistent and widely varies from one point of the sheet to another. For example, if 0.062 is assumed for its dielectric loss tangent value instead of 0.025, the experimental power loss could actually be in agreement with the predicted value when defocusing is compensated (Figure 13). Another approach to reduce impedance mismatch is to design the device with the gradient index at boundaries fading down to 1 so as to establish an adiabatic transition. However, since the starting gradient is different along the boundary inside the lens, this approach would require much more complicated design and techniques to handle multi-directional field generated alongside the material.

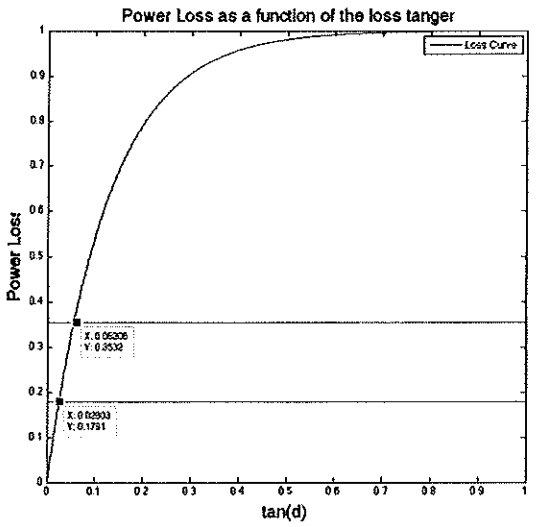

Figure 13: Power loss of Maxwell lens as a function of tan(d)

IV. Conclusion and Future Work

To design an advanced electromagnetic device, the field distribution of an existing optical device, fish-eyed lens, is modeled and distorted using a coordinate transformation that yields values of electrical permittivity and magnetic permeability. The complexity of these tensor elements is minimized using the quasi-conformal transformation optics technique, thereby obtaining a set of non-extreme isotropic index distribution characterizing the transformed region containing the device. This device, named Maxwell lens, is implemented using metamaterials, and its behaviors are confirmed at RF wavelengths with analysis that inspects the field distribution of the entire region as well as the cross-sectional power distributions at the lens boundaries. Upon successful implementation of transformation optics in combination with metamaterials, the study shows the possible applications of the flattened fish-eyed lens in such areas as photonics and chip-integrated systems. Future research remains to demonstrate the applicability of this design further in a different set of wavelengths such as IR, which can have a direct impact on the design of such waveguides as SOI(silicon-on-insulator) that constitute important part of integrated-chip designs.

V. Acknowledgement

I would like to thank Dr. David Smith and every member of the research group for giving me an opportunity to join the team and get an invaluable experience learning to apply knowledge in the innovative field of metamaterials. Also, I would like to thank John Hunt for his thoughtful guidance and tremendous support throughout the life of this research.

VI. References

[1] R. A. Shelby, D. R. Smith, and S. Schultz, "Experimental Verification of a Negative Index of Refraction," *Science* 292, 77 (2001)

[2] Jessie Y. Chin, Jonah N. Gollub, Jack J. Mock, Ruopeng Liu, Cameron Harrison, David R. Smith, and Tie Jun Cui, "An efficient broadband metamaterial wave retarder," *Opt. Express* 17, 7640-7647 (2009)

[3] W. X. Jiang, T. J. Cui, Q. Cheng, J. Y. Chin, X. M. Yang, R. P. Liu, D. R. Smith, "Design of arbitrarily shaped concentrators based on conformally optical transformation of nonuniform rational B-spline surfaces," *Applied Physics Letters* 92 264101 (2008)

[4] W. Li, J. Guan, W. Wang, "Homogeneous-materials-constructed electromagnetic field concentrators with adjustable concentrating ratio," *J. Phys. D: Appl. Phys.* 44 125401 (2011)

[5] W. Tong, H.S. Chua, Z. Hu, P.D. Curtis, A.P. Gibson, and M. Missous, "Fully Integrated Broadband CPW Left-Handed Metamaterials Based on GaAs Technology for RF/MMIC Applications," *Microwave and Wireless Components Letters, IEEE* 17, 8 (2007)

[6] H.S. Chua, P. Curtis, W. Tong, Z.R. Hu, A.P. Gibson, and M. Missous, "Integrated Left-Handed Metamaterials on MMIC Technology," *European Microwave Integrated Circuits Conference* 1st, 449-451 (2006)

[7] D. R. Smith, Y. Urzhumov, N. B. Kundtz, and N. I. Landy, "Enhancing imaging systems using transformation optics," *Opt. Express* 18, 21238-21251 (2010)

[8] N. I. Landy and W. J. Padilla, "Guiding light with conformal transformations," Opt. Express 17, 14872-14879 (2009)

[9] D. Schurig, J. J. Mock, B. J. Justice, S. A. Cummer, J. B. Pendry, A. F. Starr, and D. R. Smith, "Metamaterial Electromagnetic Cloak at Microwave Frequencies," *Science* 314, 977-980 (2006)

[10] J. B. Pendry, D. Schrig, and D. R. Smith, "Controlling Electric Magnetic Fields," *Science* 312, 1780-1782 (2006)

[11] D. Schurig, J. B. Pendry, and D. R. Smith, "Calculation of material properties and ray tracing in transformation media," *Opt. Express* 14, 9794-9804 (2006)

[12] Liu, R., Cui, T. J., Huang, D., Zhao, B. & Smith, D. R. "Description and explanation of electromagnetic behaviors in artificial metamaterials based on effective medium theory," *Phys. Rev. E* 76, 026606 (2007)

[13] D. Schurig, J. B. Pendry, and D. R. Smith, "Transformation-designed optical elements," Opt. Express 15, 14772-14782 (2007)

VII. Appendix

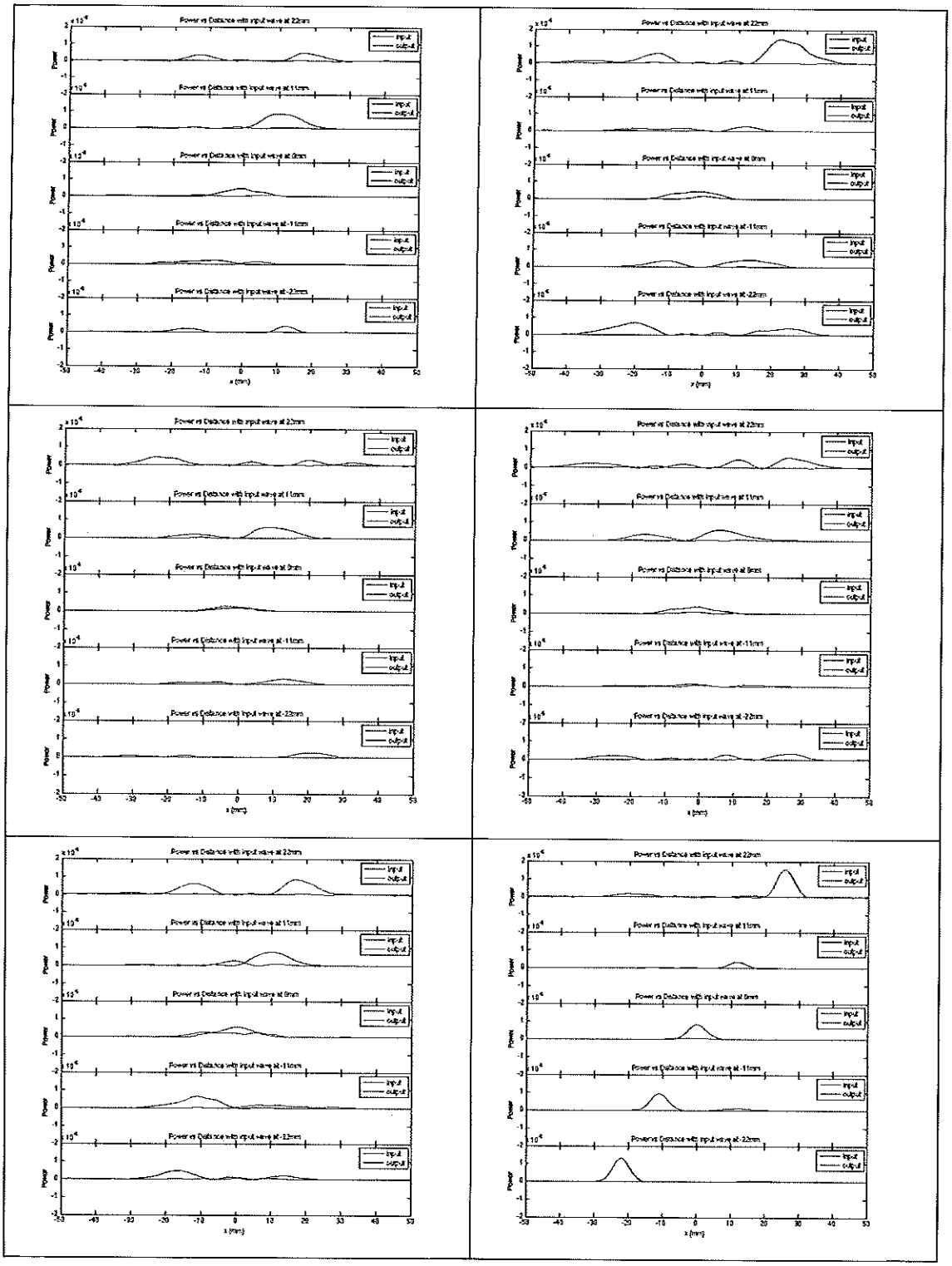

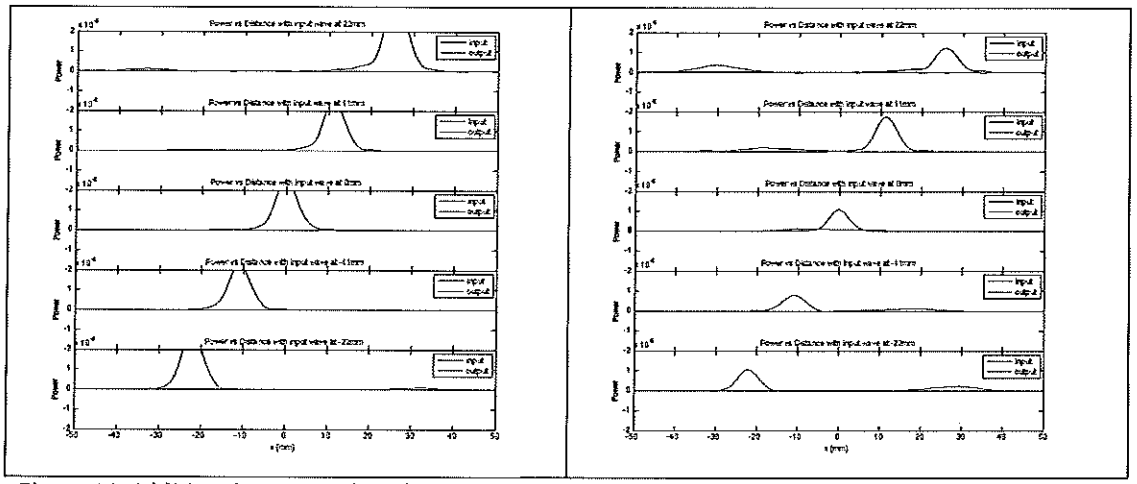

Figure 14: Additional Cross Section Plots